HHS Public Access

Author manuscript

Sci Transl Med. Author manuscript; available in PMC 2018 May 09.

Published in final edited form as:

Sci Transl Med. 2014 April 30; 6(234): 234ra58. doi:10.1126/scitranslmed.3008085.

An Acellular Biologic Scaffold Promotes Skeletal Muscle Formation in Mice and Humans with Volumetric Muscle Loss

Brian M. Sicari[1,2,*], **J. Peter Rubin**[1,3,4,*], **Christopher L. Dearth**[1,2], **Matthew T. Wolf**[1,4], **Fabrisia Ambrosio**[1,5], **Michael Boninger**[1,4,5], **Neill J. Turner**[1,2], **Douglas J. Weber**[4,5], **Tyler W. Simpson**[5], **Aaron Wyse**[6], **Elke H. P. Brown**[5], **Jenna L. Dziki**[1,4], **Lee E. Fisher**[5], **Spencer Brown**[1,3], and **Stephen F. Badylak**[1,2,†]

[1]McGowan Institute for Regenerative Medicine, University of Pittsburgh, Pittsburgh, PA 15219, USA

[2]Department of Surgery, University of Pittsburgh, Pittsburgh, PA 15219, USA

[3]Department of Plastic Surgery, University of Pittsburgh, Pittsburgh, PA 15219, USA

[4]Department of Bioengineering, University of Pittsburgh, Pittsburgh, PA 15219, USA

[5]Department of Physical Medicine & Rehabilitation, University of Pittsburgh, Pittsburgh, PA 15219, USA

[6]Department of Radiology, University of Pittsburgh, Pittsburgh, PA 15219, USA

Abstract

Biologic scaffolds composed of naturally occurring extracellular matrix (ECM) can provide a microenvironmental niche that alters the default healing response toward a constructive and functional outcome. The present study showed similarities in the remodeling characteristics of xenogeneic ECM scaffolds when used as a surgical treatment for volumetric muscle loss in both a preclinical rodent model and five male patients. Porcine urinary bladder ECM scaffold implantation was associated with perivascular stem cell mobilization and accumulation within the

†Corresponding author. badylaks@upmc.edu.
*These authors contributed equally to this work.

Competing interests: Since completion of the clinical study, S.F.B. has received honoraria from ACell Inc. for seminars. The other authors declare that they have no other competing interests.

SUPPLEMENTARY MATERIALS

www.sciencetranslationalmedicine.org/cgi/content/full/6/234/234ra58/DC1

Methods

Fig. S1. CMAP at different stimulation intensities in mice.

Fig. S2. Histomorphology in human subjects with VML.

Table S1. Semiquantification of histological findings from the mouse model of VML.

Table S2. Patient exclusion and inclusion criteria.

Reference (44)

Author contributions: S.F.B. and J.P.R. designed the human patient treatment protocol; S.F.B. obtained funding; J.P.R. performed the surgical procedures for the human patients. S.F.B. and B.M.S. designed the pre-clinical study, and B.M.S. and M.T.W. performed the surgical procedures; M.T.W., B.M.S., T.W.S., D.J.W., and L.E.F. performed EMG testing. B.M.S. and J.L.D. performed immunolabeling. A.W. performed the imaging and biopsies for the clinical study; F.A., E.H.P.B., and M.B. performed the screening physical therapy clinical exam, identified impairment and functional outcome variables, and performed evaluations; N.J.T., C.L.D., and B.M.S. collected the muscle biopsies; B.M.S. and N.J.T. performed and analyzed the immunolabeling experiments; S.F.B., C.L.D., B.M.S., M.T.W., N.J.T., F.A., and A.W. wrote the manuscript; and F.A., S.F.B., M.B., E.H.P.B., S.B., C.L.D., J.P.R., B.M.S., M.T.W., N.J.T., and A.W. revised the paper.

site of injury, and de novo formation of skeletal muscle cells. The ECM-mediated constructive remodeling was associated with stimulus-responsive skeletal muscle in rodents and functional improvement in three of the five human patients.

INTRODUCTION

Skeletal muscle accounts for more than 40% of the body's mass (1, 2) and, unlike most other tissues in the adult mammal, has the inherent ability to regenerate after injury (3–5). However, the regenerative response fails when a large volume of muscle is lost as a result of trauma [that is, volumetric muscle loss (VML)] (6), and the default outcome is scar tissue formation (7–11). Treatment options for VML are limited and include scar tissue debridement and/or muscle transposition, both of which are typically associated with morbidity and unfavorable outcomes (12–14).

Skeletal muscle regeneration relies in large part upon the activation, proliferation, migration, and differentiation of the canonical muscle stem cell, termed the satellite cell, within a conducive and permissive microenvironmental niche (3, 7). Other stem/progenitor cell populations, such as perivascular stem cells [PVSCs; $CD146^+$, neurogenin 2–positive ($NG2^+$)], have been shown to play important roles in skeletal muscle regeneration (8–11). The response of skeletal muscle to injury is critically dependent on the innate immune response, particularly the recruitment, accumulation, activation, and temporal polarization of macrophages (15). Finally, the extracellular matrix (ECM) of all tissues largely defines the microenvironmental niche and modulates the migration, behavior, and phenotype of resident cells during development and homeostasis and in response to injury (16–19). Although most regenerative medicine strategies to address the loss of muscle mass have been cell-centric, the present study describes an acellular approach that is based on use of an ECM biologic scaffold to provide a supportive microenvironmental niche that influences endogenous cell behavior at the site of interest.

Surgical placement of acellular biologic scaffold materials composed of mammalian ECM promotes a constructive, functional skeletal muscle response after experimentally induced skeletal muscle injury in small (20–23) and large (24) animal models. There is also an anecdotal report of the use of an ECM scaffold in a human patient after extremity trauma with VML (25). This ECM-mediated response occurs by mechanisms thought to include the recruitment of stem/progenitor cells via the formation of chemotactic cryptic peptides (26–28) and modulation of macrophage phenotype (29–31).

Here, we report the use of a recently described rodent model of VML to evaluate the effect of a urinary bladder ECM biologic scaffold upon the healing response and functional outcome (20). Results show the presence of PVSCs both surrounding neovasculature and spatially distinct from vascular structures during the process of ECM scaffold remodeling. ECM-treated defects also showed the formation of de novo skeletal muscle fibers and associated functional improvement. In a parallel human clinical study, five patients suffering from extremity VML were treated with an ECM biologic scaffold and showed not only a similar presence and distribution of PVSCs with associated de novo formation of skeletal

muscle as observed in the rodent model but also functional improvement in three of the five patients.

RESULTS

Biologic scaffolds for the treatment of VML in a mouse model

A recently described murine model of VML (20) was used to evaluate the spatial and temporal presence of endogenous PVSCs and skeletal muscle cells during the remodeling of biologic scaffolds at the site of skeletal muscle injury. Specifically, in this model of VML, a critical size excisional defect was created in the quadriceps compartment of the mouse hindlimb. In uninjured, normal mouse skeletal muscle, PVSCs ($CD146^+NG2^+$ cells) were identified by immunolabeling within their native perivascular anatomic location around von Willebrand factor–positive (vWF^+) capillaries and arterioles (Fig. 1A).

PVSCs remained within their normal vascular-associated niche in both untreated VML defects and those implanted with a porcine urinary bladder ECM biologic scaffold at 7 days after injury and scaffold implantation (Fig. 1A). However, at 14 days after injury, untreated defects continued to show vascular-associated PVSCs, whereas defects treated with ECM showed PVSCs outside their normal perivascular niche and in the midst of the degrading ECM scaffold material (Fig. 1A). At 6 months after injury, the untreated VML defects showed no signs of new skeletal muscle formation, whereas defects treated with ECM showed the formation of islands of $desmin^+$ and myosin heavy chain–positive (MHC^+) striated skeletal muscle throughout the area of scaffold placement (table S1), consistent with an ECM-mediated constructive remodeling effect (Fig. 1B). A semiquantitative analysis of PVSCs, angiogenesis, and $desmin^+/MHC^+$ skeletal muscle cells present in the defects at 7 days, 14 days, and 6 months after injury is provided in table S1.

Electromyography of innervated muscle within remodeled tissue in mice

Electromyographic (EMG) analysis was conducted to quantify and characterize functionally innervated muscle fibers present within the remodeling ECM placement site at 180 days after treatment in the murine VML model. The EMG electrodes were placed within areas of remodeled tissue and insulated from surrounding healthy muscle (Fig. 2A). After nerve stimulation, ECM-treated VML defects showed muscle activation characteristics that were more similar to that of uninjured muscle than to untreated defects. Muscle fibers were recruited more rapidly with a greater peak-to-peak voltage (V_{PP}) response when compared to untreated defects (Fig. 2B). Furthermore, the untreated VML injury resulted in reduced maximal peak-to-peak voltage ($V_{PP\text{-}max}$) and root mean square voltage ($V_{RMS\text{-}max}$) compared to ECM-treated defects (Fig. 2C), which is indicative of decreased muscle fiber recruitment.

Greater stimulation intensities were required to evoke the threshold (S_{thresh}), half-maximal ($S_{1/2}$), and maximal (S_{max}) EMG response in injured animals than in uninjured (healthy) animals, but this stimulation intensity requirement was partially rescued by treatment with ECM (Fig. 2D). The rate of muscle fiber recruitment after the threshold stimulation (that is, the slope of the recruitment curve) also decreased in injured animals, which was partially

restored by treatment with ECM (Fig. 2E). ECM treatment positively affected each of the EMG parameters in Fig. 2 compared to untreated VML animals, except for S_{max} (Fig. 2D).

Representative waveforms of the compound muscle action potential (CMAP) at different stimulation intensities are shown in fig. S1 (A to C). Increasing stimulation intensities up to 2.0 V in uninjured muscle correlates with additional muscle fiber recruitment and a corresponding increase in CMAP amplitude, whereas untreated defects at the same stimulation produce a negligible response. ECM treatment, in contrast, is stimulated at similar intensities to uninjured tissue, resulting in similar CMAP amplitudes. Furthermore, β-III tubulin immunolabeling showed the presence of neurons within the remodeled ECM scaffold implantation sites (fig. S1D).

Pre- and postsurgical physical therapy and imaging in patients

A cohort study examining outcomes after reconstruction of VML with porcine urinary bladder ECM in five human patients (Table 1) was conducted (Fig. 3A) following the encouraging results in the rodent model. All subjects were male and at least 6 months removed from the time of injury. In accordance with the established inclusion criteria (table S2), all subjects showed a minimum of 25% functional and structural deficit compared to the contralateral limb. All participants had previously been subjected to multiple surgical procedures and extensive physical therapy, and thus were considered to have exhausted all available standard of care options.

Each patient was prescribed to a custom-designed physical therapy regimen lasting between 12 and 26 weeks, during which time they plateaued with respect to their functional ability. The subsequent surgical procedure involved excision of local scar tissue, identification of adjacent vascularized and innervated muscle tissue, and placement of an acellular biologic scaffold material composed of porcine urinary bladder ECM. Each patient was then placed in their respective physical therapy program within 48 hours after surgery (Fig. 3A).

Presurgical imaging was performed and repeated postsurgically after physical therapy at about 6 months for each subject (Fig. 3A). Four of the five subjects were examined using a 1.5-T magnetic resonance imaging (MRI) scanner, whereas one subject was imaged by computed tomography (CT) scanning because of retained shrapnel fragments and indwelling metallic hardware. The presurgical estimated volume of lost muscle ranged from 58 to 90% of contralateral limb musculature (Table 1). Characterization of the location and appearance of the ECM scaffold as well as a change in volume or appearance of the surrounding soft tissue were performed on the postsurgical imaging. When comparing pre- versus post-scaffold implantation, MR or CT imaging of the injured limb showed the formation of dense tissue, consistent with skeletal muscle at the implantation site at about 6 months after surgery (Fig. 3B).

Histomorphology in human subjects with VML

Patients were biopsied at two time points after surgery (Fig. 3A). Representative images from each patient showing PVSCs and vessels in 6- to 8-week biopsies and desmin$^+$ skeletal muscle cells in 6-month biopsies are found in fig. S3. At 5 to 8 weeks after implantation of the ECM scaffold, the histomorphologic characteristics were similar for all five patients and

showed a mononuclear cell infiltrate of variable density. Neocapillaries and arterioles, identified by vWF staining, were present in all specimens (Table 2 and fig. S3). Randomly scattered $CD146^+NG2^+$ PVSCs were both associated with vWF^+ vascular structures and independent of any vascular structures in all patients, except for patient 4 (Fig. 4A, Table 2, and fig. S2). Islands of centrally nucleated $desmin^+$ and MHC^+ cells that were not associated with any vascular structure were present in biopsy specimens from patients 3 and 5 at 5 to 8 weeks (Fig. 4B and Table 2) but not in biopsy specimens from any of the other patients.

At 6 to 8 months after surgery (24 to 32 weeks), all five patients treated with surgically placed ECM showed similar histologic findings at the scaffold placement site. $CD146^+$ PVSCs were again identified both associated with vWF^+ vascular structures and independent of any vascular structures in all patients (Fig. 4A and Table 2). $Desmin^+$ and MHC^+ cells with central nuclei—indicative of actively regenerating skeletal muscle cells—and new mature skeletal muscle cells were seen in biopsy samples from all patients either as individual cells or in variably sized clusters of cells (Fig. 4B, fig. S3, and Table 2). Areas not occupied by new skeletal muscle were characterized by abundant small blood vessels within the moderately organized connective tissue. No recognizable scaffold material was present in any of the biopsy specimens.

Postsurgical function in VML patients

At 24 to 28 weeks after surgery, the subjects showed an average increase of about 25 and 220% in force production and functional tasks (that is, activities of daily living), respectively (Tables 3 and 4). Three of the five patients showed 20% or greater improvement of strength (range, 20 to 136%) of the affected limb 6 months after surgery (Table 3). The two subjects diagnosed with anterior compartment syndrome that were unable to produce any measureable force production before the surgical manipulation showed no improvement in strength throughout the duration of the study (patients 1 and 2); yet, a third subject (patient 5) with the same diagnosis who retained some presurgical dorsiflexion strength (3.6 lb as determined by a handheld dynamometer) showed a 33% improvement in strength 6 months after surgery (Fig. 5, A and B).

Six months after surgery, three of five subjects showed improvement in the functional outcome variables (Table 4). Both individuals receiving ECM transplantation into the quadriceps region showed improvements in functional capacity. Patient 3 showed a marked improvement (1820%) in the single hop test at 6 months after surgery. Patient 4 showed improvements in the chair lift test (324%) and max single leg squats (417%). Of the individuals receiving ECM transplantation to the anterior compartment, patient 1 did not show any functional improvement 6 months after surgery, whereas patients 2 and 5 both showed an improvement in balance measures as determined by single leg stance time with eyes closed and the backward reach test (Fig. 5D).

DISCUSSION

The work described here shows the remodeling potential of an acellular ECM bioscaffold for restoration of skeletal muscle both in a pre-clinical rodent model and in patients with VML. Using an established model of VML (20), we demonstrate that an acellular scaffold

composed of porcine ECM can promote formation of new muscle tissue in vivo in mice and in humans. In mice, we identified a central role for PVSCs in this process and noted the presence of skeletal muscle cells after ECM implantation after 6 months. These findings were corroborated by the histomorphologic results from the human study. Implantation of ECM at the site of injury was associated with neovascularization, the mobilization and accumulation of PVSCs, myogenesis, and functional recovery in both the preclinical and clinical studies. Specifically, functional improvement surpassing that achieved by physical therapy alone was obtained in three of five patients.

Most strategies for restoration or de novo formation of skeletal muscle tissue depend on the use of cells and typically involve the delivery of exogenous cells to sites of injured or missing tissue (32–34). These cell-based strategies have been largely ineffective for several reasons, including immunogenicity, inefficient methods of delivery, and apoptosis after delivery (35, 36). It is now generally accepted that delivered cells most likely exert therapeutic effects via paracrine-mediated mechanisms (37, 38). An acellular approach, which has the potential to recruit endogenous host cells, such as that used in the present study, obviates limitations associated with the delivery of exogenous cells.

Both rodent and patient biopsies showed PVSCs removed from their normal vessel-associated anatomic location, in the midst of partially degraded ECM scaffold material, suggesting that these cells participate in the remodeling of the ECM scaffold. Histologic findings show the appearance of both immature and mature desmin$^+$ and MHC$^+$ skeletal muscle cells within the implantation site. Patient biopsies collected from sites of VML had formed soft tissue after 6 months—consistent with skeletal muscle—as identified by either MRI or CT and confirmed with immunolabeling. In three of five subjects, the histologic and imaging findings were concomitant with functional improvement. PVSCs contribute to de novo skeletal muscle formation not only during fetal development but also in adult tissue in response to acute injury (39). Therefore, it is plausible that the PVSCs contributed to the formation of skeletal muscle in the present studies, either directly through terminal myogenic differentiation or indirectly through paracrine mechanisms. The contribution of alternative sources of precursor cells from the adjacent healthy muscle tissue and/or resident or circulating mesenchymal stem cells, including satellite cells, cannot be ruled out (36).

Two aspects of the protocol by which the five patients in the present report were treated are of particular note. First, the patients were all well past the acute injury response phase and had been subjected to multiple surgical procedures that included debridement and/or tenolysis as dictated by standard of care. All previous procedures in these patients proved less than satisfactory and resulted in compromised activities of daily living. Therefore, it is unlikely that the improvement noted after ECM treatment was part of a delayed natural healing response or the result of debridement at the time of ECM implantation. Second, all five patients completed a presurgical, customized, intense physical therapy program that focused specifically on their individual functional deficits. The identification and maximization of functional parameters before surgery and the use of these optimized parameters as baseline measures for postoperative metrics minimize the likelihood that any improvement after ECM intervention was solely the result of the physical therapy component of care. Stated differently, because each patient underwent a documented plateau

in physical performance before ECM implantation, it is unlikely that any increase in muscle mass of the treated compartment or improvement in function was due to hypertrophy of the native muscle.

ECM treatment facilitated increased muscle activity in the mouse VML model as shown with EMG testing, which shows the presence of electrically active, functionally innervated myofibers within the defect area. ECM treatment resulted in a marked improvement in muscle recruitment parameters compared to untreated VML defects, although it did not fully approximate normal skeletal muscle. The increase in maximal EMG amplitude in ECM-treated animals suggests recruitment of a greater number of myofibers in the defect area (40) compared to untreated animals. Reduced threshold stimulation intensity and an increase in recruitment rate may provide insights into properties of the innervating motor neurons. Large-diameter neurons have lower stimulation thresholds than smaller-diameter neurons, whereas the average motor unit size influences fiber recruitment rate (40). Both parameters are more similar to healthy muscle after ECM treatment than in untreated animals. An increased threshold might also be due to a reduced number of myofibers per motor unit, and a corresponding decrease in the EMG signal, resulting in the requirement of a larger stimulus to produce a detectable response (41). Note that EMG does not necessarily linearly correlate with muscle strength or stability. EMG provides a sensitive characterization of muscle fiber activity that is dependent on several functional factors such as nerve conduction properties and neuromuscular junction activity. EMG is not an indication of fiber force production or whether fibers are optimally oriented and mechanically coupled (42). Nevertheless, these data show that multiple aspects of the muscle recruitment pattern were altered by ECM treatment, suggesting that cell types other than myofibers (for example, neurons) are involved in ECM remodeling.

The results reported here show similarities in the cellular remodeling characteristics between a pre-clinical rodent model and the clinical application of ECM scaffolds for the treatment of VML. However, limitations of this study should be noted. In mice, after 6 months, untreated VML defects showed the hallmarks of default mammalian wound healing including the formation of scar tissue, the lack of any notable skeletal muscle cell presence, and the associated lack of EMG response. Conversely, ECM-treated VML defects were characterized by abundant cellularity, angiogenesis, the onset of skeletal muscle formation, and an associated increase in EMG response when compared to untreated defects. Although the preclinical model allowed inclusion of an untreated control group, this was not possible in the clinical study. For example, the impact of the excision of scar tissue and tenolysis, when performed, cannot be assessed as an independent variable. Furthermore, associated placebo effects (that is, patients may have had more confidence in their treated leg after implantation, which may have affected functional outcomes) were unable to be controlled. Some biologic scaffolds are commonly used in clinical practice to promote host tissue ingrowth, including fibrous tissue formation (43). The present study confirmed skeletal muscle tissue formation at the scaffold implantation site; however, it was not possible to directly correlate the amount of de novo skeletal muscle formation to the amount of functional improvement. The presence of host PVSCs and skeletal muscle formation within the scaffold implantation site were shown. However, it was not possible to lineage-trace the

endogenous PVSCs and show their direct contribution to de novo skeletal muscle. Therefore, the definitive precursor cell(s) to the new muscle fibers remains an open question.

Another limitation of this study is the small number of patients. Five subjects are insufficient to conduct statistical analysis of the results, which is why data are presented as a series of case studies. In a human population with a variety of injuries and mechanisms of injury, each patient is unique; no two patients will present with identical or even similar morphometrics, comorbidities, or anatomic deficits. Two of the patients were considered as nonresponders per preset study guidelines. However, given the severity and chronicity of the injury and the preoperative physical therapy, the results in three subjects are notable. Note that the two nonresponders both showed improvement in at least one functional task, and both expressed an improved quality of life. A common finding among the nonresponders was lack of active movement across the weakened joint.

The present study describes an acellular approach that results in the de novo formation of skeletal muscle. ECM scaffolds have been shown to provide an inductive niche that facilitates the recruitment and differentiation of endogenous myogenic progenitor cells (24, 26). Directed mobilization of relevant endogenous cell sources obviates the need for exogenous cell administration and removes the associated cell harvesting procedures, regulatory barriers, and any potential cell-related immune responses. This translational work shows that ECM scaffolds may serve as inductive scaffolds that promote remodeling of muscle tissue in VML. The clinical translation of this acellular approach for restoration of skeletal muscle in patients with VML is promising, and the concept of providing an inductive niche that can alter the default scar tissue response to injury is worthy of further study.

MATERIALS AND METHODS

Study design

Preclinical studies—A mouse model of VML was used to examine the ability of biologic scaffolds composed of ECM to promote site-appropriate formation of functional skeletal muscle tissue. Institutional Animal Care and Use Committee (IACUC)–approved surgical procedures involved the creation of a critically sized, unilateral excisional defect in the quadriceps hindlimb musculature. Animals were randomized into treatment groups, and defects were either left untreated ($n = 4$ per time point) or treated with surgically placed biologic scaffolds composed of ECM ($n = 4$ per time point). All analyses were carried out in blinded fashion. Histological analysis was used to identify vasculature structures at 7 and 14 days after surgery and skeletal muscle at 6 months after surgery. The presence of innervated skeletal muscle tissue was evaluated by EMG at the 6-month time point ($n = 8$). Animal numbers were selected on the basis of previous studies.

Clinical case studies—A clinical study examining outcomes after reconstruction of VML with ECM was conducted with informed patient consent and approvals from the Institutional Review Board of the University of Pittsburgh and the U.S. Department of Defense Human Research Protection Office (ClinicalTrials.gov identifier: NCT01292876). A schematic of the clinical cohort study design is shown in Fig. 3A. Briefly, patients were

screened against established exclusion and inclusion criteria (table S2). Five were enrolled and subjected to physical therapy. All patients received the acellular implant. MR and CT imaging were used to quantify muscle tissue before and 6 months after surgery. All analyses were conducted in blinded fashion, and positive patient responders were defined by a 25% or greater increase over their presurgical functional maximum.

Mouse model of VML

Experimental design, scaffold preparation, surgical procedure, and tissue harvest were performed as previously described (20). Briefly, approval was obtained from the University of Pittsburgh IACUC. Twenty-four female C57BL/6 mice were randomly assigned into either treated or untreated experimental groups. Both groups were subjected to a muscle defect consisting of unilateral resection of the tensor fascia latae quadriceps muscle. The VML defect accounts for a loss of about 90% of the fascia latae and 60% of the rectus femoris. In total, the defect represents a volumetric loss of about 75% of the quadriceps skeletal muscle compartment. This 75% loss is analogous to the VML injuries treated in the translational portion of the present manuscript. The defects within the treated group were filled with a biologic scaffold composed of ECM. Nonresorbable marker sutures were placed at the corners of the defect in both groups and were used to identify the defect margins. The time points for evaluation were 7, 14, and 180 days ($n = 4$ per time point per group). Microscopic analysis included histochemistry and immunolabeling to examine PVSCs and skeletal muscle tissue.

EMG of remodeled tissue in the mouse model

EMG was performed to evaluate the CMAP of functionally innervated muscle within the mouse VML defect after 180 days, as described in Supplementary Methods.

Patient selection and screening examination

A minimum of 6 months from the time of injury and age between 18 and 70 years were inclusion criteria (table S2) for experimental surgical intervention with the ECM scaffold approach. In addition, a minimum of 25% loss of muscle mass as determined by MRI or CT and a documented minimum loss of 25% function, compared to the contra-lateral muscle group, were required. Innervation to existing musculature within the injured compartment was considered to be necessary for a positive outcome and was confirmed before surgical procedure on the basis of EMG testing. Exclusion criteria (table S2) included open wounds or active infection at the site of injury, bleeding disorders, medical comorbidities that would impair wound healing, and inability to comply with physical therapy. Informed consent was obtained after the nature and possible consequences of the study were explained.

Physical therapy

After enrollment, patients were first entered into a custom-designed physical therapy program on the basis of their specific muscle deficit to optimize function. The ability to perform tasks that quantified the function of the injured/missing muscle tissue was tracked during the pre-surgical training period until a plateau was reached and no additional measurable progress could be obtained for a minimum of 2 weeks—that is, maximum

function was reached with optimal physical therapy (Fig. 3A, blue ramp progression). Detailed physical therapy screening evaluation and pre- and postsurgical physical therapies are described in Supplementary Methods.

Surgical procedure

Procedures were performed under general anesthesia in a tertiary care medical center. Through an open incision, sharp debridement of scar tissue was performed, along with selective tenolysis. The injured muscle compartment was reconstructed with the ECM device (MatriStem, ACell Inc.). The scaffold material consisted of eight layers of urinary bladder ECM laminated by vacuum pressing into a sheet configuration and measuring about 4 mm in thickness. The ECM scaffold was implanted within the VML injury site, with maximal surface contact adjacent to native healthy tissue, and secured under moderate tension with either permanent or slowly absorbing sutures. Range of motion was then evaluated to ensure that the graft was secure. Care was taken to avoid contact of the scaffold with bone, and all empty space was obliterated before closure of the surgical site to ensure maximal contact of the scaffold with host soft tissue on all surfaces. Closed suction drains were placed in most cases before closure of the subcutis with absorbable sutures.

MR and CT imaging

The MRI protocols included a variety of sequences in sagittal, coronal, and axial planes using T1-weighted spin echo, T2-weighted fast spin echo with or without fat suppression, and STIR sequences. The CT imaging protocol included unenhanced axial image acquisition at a slice thicknesses of 1.25 and 2.5 mm with both soft tissue and bone kernels. Optimal imaging parameters were 120 kVp and 240 mA. The images were volumetrically reformatted into coronal and soft tissue planes.

Imaging was reviewed by a musculoskeletal-trained radiologist. Pre-surgical MRI was assessed for degree of loss of normal muscle bulk, muscle signal abnormality including presence or absence of fatty infiltration and denervation edema, integrity of the musculotendinous units (when possible), presence of concomitant fascial injury, and characterization of previous postsurgical and/or posttraumatic changes. Presurgical CT imaging was assessed for similar features, with characterization of muscular attenuation replacing characterization of muscle signal abnormality. Characterization of the location and appearance of the ECM scaffold as well as a change in volume or appearance of the surrounding musculature were performed on the postsurgical imaging.

Tissue biopsy

Ultrasound-guided needle biopsies were taken from the scaffold implantation site on two separate occasions: 5 to 8 weeks after surgery and again at 24 to 32 weeks after surgery. The biopsies spanned the full length (that is, proximal to distal) and width (that is, medial to lateral) of the scaffold implantation site and ranged in number from 6 to 9. The specimens were snap-frozen with liquid nitrogen and stored at −80°C for subsequent immunolabeling studies (Supplementary Methods).

Statistical analysis

For the EMG data analysis, all values are presented as means ± SE ($n = 7$). Statistical analysis of S_{thresh}, $S_{1/2}$, S_{max}, and slope was conducted with a Kruskal-Wallis nonparametric ANOVA with a post hoc Mann-Whitney U test and Sidak correction using SPSS software (IBM SPSS Statistics v21, IBM Inc.). Statistical significance was defined as $P < 0.05$. Significant differences between healthy muscle tissue and ECM or untreated defects were denoted with * or #, respectively.

Supplementary Material

Refer to Web version on PubMed Central for supplementary material.

Acknowledgments

The U.S. Department of Defense's Limb Salvage and Regenerative Medicine Initiative and the Muscle Tendon Tissue Unit Repair and Reinforcement Reconstructive Surgery Research study is collaboratively managed by the Office of the Secretary of Defense. The Initiative is focused on rapidly and safely transitioning advanced medical technology in commercially viable capabilities to provide our wounded warriors the safest and most advanced care possible today.

Funding: Supported by research grants to S.F.B. and J.P.R. by the U.S. Department of the Interior, National Business Center, Acquisition Services Directorate, Sierra Vista Branch (award no. D11AC00006). A. Russell was instrumental in the acquisition of this funding. B.M.S. was supported by NIH grant F31AG042199. M.T.W. was partially supported by the NIH–National Heart, Lung, and Blood Institute training grant (T32-HL76124-6) entitled "Cardiovascular Bioengineering Training Program" through the University of Pittsburgh Department of Bioengineering.

REFERENCES AND NOTES

1. Huard J, Li Y, Fu FH. Muscle injuries and repair: Current trends in research. J Bone Joint Surg Am. 2002; 84-A:822–832. [PubMed: 12004029]
2. Yin H, Price F, Rudnicki MA. Satellite cells and the muscle stem cell niche. Physiol Rev. 2013; 93:23–67. [PubMed: 23303905]
3. Chargé SB, Rudnicki MA. Cellular and molecular regulation of muscle regeneration. Physiol Rev. 2004; 84:209–238. [PubMed: 14715915]
4. Järvinen T, Järvinen TL, Kääriäinen M, Kalimo H, Järvinen M. Muscle injuries: Biology and treatment. Am J Sports Med. 2005; 33:745–764. [PubMed: 15851777]
5. Carlson BM, Faulkner JA. The regeneration of skeletal muscle fibers following injury: A review. Med Sci Sports Exerc. 1983; 15:187–198. [PubMed: 6353126]
6. Grogan BF, Hsu JR. Skeletal Trauma Research Consortium. Volumetric muscle loss. J Am Acad Orthop Surg. 2011; 19(Suppl 1):S35–S37. [PubMed: 21304045]
7. Mauro A. Satellite cell of skeletal muscle fibers. J Biophys Biochem Cytol. 1961; 9:493–495. [PubMed: 13768451]
8. Crisan M, Yap S, Casteilla L, Chen CW, Corselli M, Park TS, Andriolo G, Sun B, Zheng B, Zhang L, Norotte C, Teng PN, Traas J, Schugar R, Deasy BM, Badylak S, Buhring HJ, Giacobino JP, Lazzari L, Huard J, Péault B. A perivascular origin for mesenchymal stem cells in multiple human organs. Cell Stem Cell. 2008; 3:301–313. [PubMed: 18786417]
9. LaBarge MA, Blau HM. Biological progression from adult bone marrow to mononucleate muscle stem cell to multinucleate muscle fiber in response to injury. Cell. 2002; 111:589–601. [PubMed: 12437931]
10. Palermo AT, Labarge MA, Doyonnas R, Pomerantz J, Blau HM. Bone marrow contribution to skeletal muscle: A physiological response to stress. Dev Biol. 2005; 279:336–344. [PubMed: 15733662]

11. Ten Broek RW, Grefte S, Von den Hoff JW. Regulatory factors and cell populations involved in skeletal muscle regeneration. J Cell Physiol. 2010; 224:7–16. [PubMed: 20232319]
12. Lin SH, Chuang DC, Hattori Y, Chen HC. Traumatic major muscle loss in the upper extremity: Reconstruction using functioning free muscle transplantation. J Reconstr Microsurg. 2004; 20:227–235. [PubMed: 15088207]
13. Leitgeb B. Structural investigation of endomorphins by experimental and theoretical methods: Hunting for the bioactive conformation. Chem Biodivers. 2007; 4:2703–2724. [PubMed: 18081108]
14. Klinkenberg M, Fischer S, Kremer T, Hernekamp F, Lehnhardt M, Daigeler A. Comparison of anterolateral thigh, lateral arm, and parascapular free flaps with regard to donor-site morbidity and aesthetic and functional outcomes. Plastic Reconstr Surg. 2013; 131:293–302.
15. Tidball JG, Villalta SA. Regulatory interactions between muscle and the immune system during muscle regeneration. Am J Physiol Regul Integr Comp Physiol. 2010; 298:R1173–R1187. [PubMed: 20219869]
16. Bissell MJ, Aggeler J. Dynamic reciprocity: How do extracellular matrix and hormones direct gene expression? Prog Clin Biol Res. 1987; 249:251–262. [PubMed: 3671428]
17. Bissell MJ, Hall HG, Parry G. How does the extracellular matrix direct gene expression? J Theor Biol. 1982; 99:31–68. [PubMed: 6892044]
18. Boudreau N, Myers C, Bissell MJ. From laminin to lamin: Regulation of tissue-specific gene expression by the ECM. Trends Cell Biol. 1995; 5:1–4. [PubMed: 14731421]
19. Ingber D. Extracellular matrix and cell shape: Potential control points for inhibition of angiogenesis. J Cell Biochem. 1991; 47:236–241. [PubMed: 1724246]
20. Sicari BM, Agrawal V, Siu BF, Medberry CJ, Dearth CL, Turner NJ, Badylak SF. A murine model of volumetric muscle loss and a regenerative medicine approach for tissue replacement. Tissue Eng Part A. 2012; 18:1941–1948. [PubMed: 22906411]
21. Wolf MT, Daly KA, Reing JE, Badylak SF. Biologic scaffold composed of skeletal muscle extracellular matrix. Biomaterials. 2012; 33:2916–2925. [PubMed: 22264525]
22. Valentin JE, Turner NJ, Gilbert TW, Badylak SF. Functional skeletal muscle formation with a biologic scaffold. Biomaterials. 2010; 31:7475–7484. [PubMed: 20638716]
23. Corona BT, Machingal MA, Criswell T, Vadhavkar M, Dannahower AC, Bergman C, Zhao W, Christ GJ. Further development of a tissue engineered muscle repair construct in vitro for enhanced functional recovery following implantation in vivo in a murine model of volumetric muscle loss injury. Tissue Eng Part A. 2012; 18:1213–1228. [PubMed: 22439962]
24. Turner NJ, Yates AJ Jr, Weber DJ, Qureshi IR, Stolz DB, Gilbert TW, Badylak SF. Xenogeneic extracellular matrix as an inductive scaffold for regeneration of a functioning musculotendinous junction. Tissue Eng Part A. 2010; 16:3309–3317. [PubMed: 20528669]
25. Mase VJ Jr, Hsu JR, Wolf SE, Wenke JC, Baer DG, Owens J, Badylak SF, Walters TJ. Clinical application of an acellular biologic scaffold for surgical repair of a large, traumatic quadriceps femoris muscle defect. Orthopedics. 2010; 33:511. [PubMed: 20608620]
26. Agrawal V, Tottey S, Johnson SA, Freund JM, Siu BF, Badylak SF. Recruitment of progenitor cells by an extracellular matrix cryptic peptide in a mouse model of digit amputation. Tissue Eng Part A. 2011; 17:2435–2443. [PubMed: 21563860]
27. Smith JG, Smith AJ, Shelton RM, Cooper PR. Recruitment of dental pulp cells by dentine and pulp extracellular matrix components. Exp Cell Res. 2012; 318:2397–2406. [PubMed: 22819733]
28. Agrawal V, Johnson SA, Reing J, Zhang L, Tottey S, Wang G, Hirschi KK, Braunhut S, Gudas LJ, Badylak SF. Epimorphic regeneration approach to tissue replacement in adult mammals. Proc Natl Acad Sci USA. 2010; 107:3351–3355. [PubMed: 19966310]
29. Sicari BM, Johnson SA, Siu BF, Crapo PM, Daly KA, Jiang H, Medberry CJ, Tottey S, Turner NJ, Badylak SF. The effect of source animal age upon the in vivo remodeling characteristics of an extracellular matrix scaffold. Biomaterials. 2012; 33:5524–5533. [PubMed: 22575834]
30. Brown BN, Badylak SF. Expanded applications, shifting paradigms and an improved understanding of host–biomaterial interactions. Acta Biomater. 2013; 9:4948–4955. [PubMed: 23099303]

31. Badylak SF, Valentin JE, Ravindra AK, McCabe GP, Stewart-Akers AM. Macrophage phenotype as a determinant of biologic scaffold remodeling. Tissue Eng Part A. 2008; 14:1835–1842. [PubMed: 18950271]
32. Huard J, Bouchard JP, Roy R, Malouin F, Dansereau G, Labrecque C, Albert N, Richards CL, Lemieux B, Tremblay JP. Human myoblast transplantation: Preliminary results of 4 cases. Muscle Nerve. 1992; 15:550–560. [PubMed: 1584246]
33. Seale P, Rudnicki MA. A new look at the origin, function, and "stem-cell" status of muscle satellite cells. Dev Biol. 2000; 218:115–124. [PubMed: 10656756]
34. Mendell JR, Kissel JT, Amato AA, King W, Signore L, Prior TW, Sahenk Z, Benson S, McAndrew PE, Rice R, Nagaraja H, Stephens R, Lantry L, Morris GE, Burghes AHM. Myoblast transfer in the treatment of Duchenne's muscular dystrophy. N Engl J Med. 1995; 333:832–838. [PubMed: 7651473]
35. Skuk D, Roy B, Goulet M, Tremblay JP. Successful myoblast transplantation in primates depends on appropriate cell delivery and induction of regeneration in the host muscle. Exp Neurol. 1999; 155:22–30. [PubMed: 9918701]
36. Péault B, Rudnicki M, Torrente Y, Cossu G, Tremblay JP, Partridge T, Gussoni E, Kunkel LM, Huard J. Stem and progenitor cells in skeletal muscle development, maintenance, and therapy. Mol Ther. 2007; 15:867–877. [PubMed: 17387336]
37. Camargo FD, Chambers SM, Drew E, McNagny KM, Goodell MA. Hematopoietic stem cells do not engraft with absolute efficiencies. Blood. 2006; 107:501–507. [PubMed: 16204316]
38. Gnecchi M, He H, Liang OD, Melo LG, Morello F, Mu H, Noiseux N, Zhang L, Pratt RE, Ingwall JS, Dzau VJ. Paracrine action accounts for marked protection of ischemic heart by Akt-modified mesenchymal stem cells. Nat Med. 2005; 11:367–368. [PubMed: 15812508]
39. Dellavalle A, Maroli G, Covarello D, Azzoni E, Innocenzi A, Perani L, Antonini S, Sambasivan R, Brunelli S, Tajbakhsh S, Cossu G. Pericytes resident in postnatal skeletal muscle differentiate into muscle fibres and generate satellite cells. Nat Commun. 2011; 2:499. [PubMed: 21988915]
40. Hegedus J, Putman CT, Gordon T. Time course of preferential motor unit loss in the SOD1^{G93A} mouse model of amyotrophic lateral sclerosis. Neurobiol Dis. 2007; 28:154–164. [PubMed: 17766128]
41. Azzouz M, Leclerc N, Gurney M, Warter JM, Poindron P, Borg J. Progressive motor neuron impairment in an animal model of familial amyotrophic lateral sclerosis. Muscle Nerve. 1997; 20:45–51. [PubMed: 8995582]
42. Warren GL, Ingalls CP, Shah SJ, Armstrong RB. Uncoupling of in vivo torque production from EMG in mouse muscles injured by eccentric contractions. J Physiol. 1999; 515(Pt. 2):609–619. [PubMed: 10050026]
43. Corona BT, Wu X, Ward CL, McDaniel JS, Rathbone CR, Walters TJ. The promotion of a functional fibrosis in skeletal muscle with volumetric muscle loss injury following the transplantation of muscle-ECM. Biomaterials. 2013; 34:3324–3335. [PubMed: 23384793]
44. Klimstra M, Zehr EP. A sigmoid function is the best fit for the ascending limb of the Hoffmann reflex recruitment curve. Exp Brain Res. 2008; 186:93–105. [PubMed: 18046545]

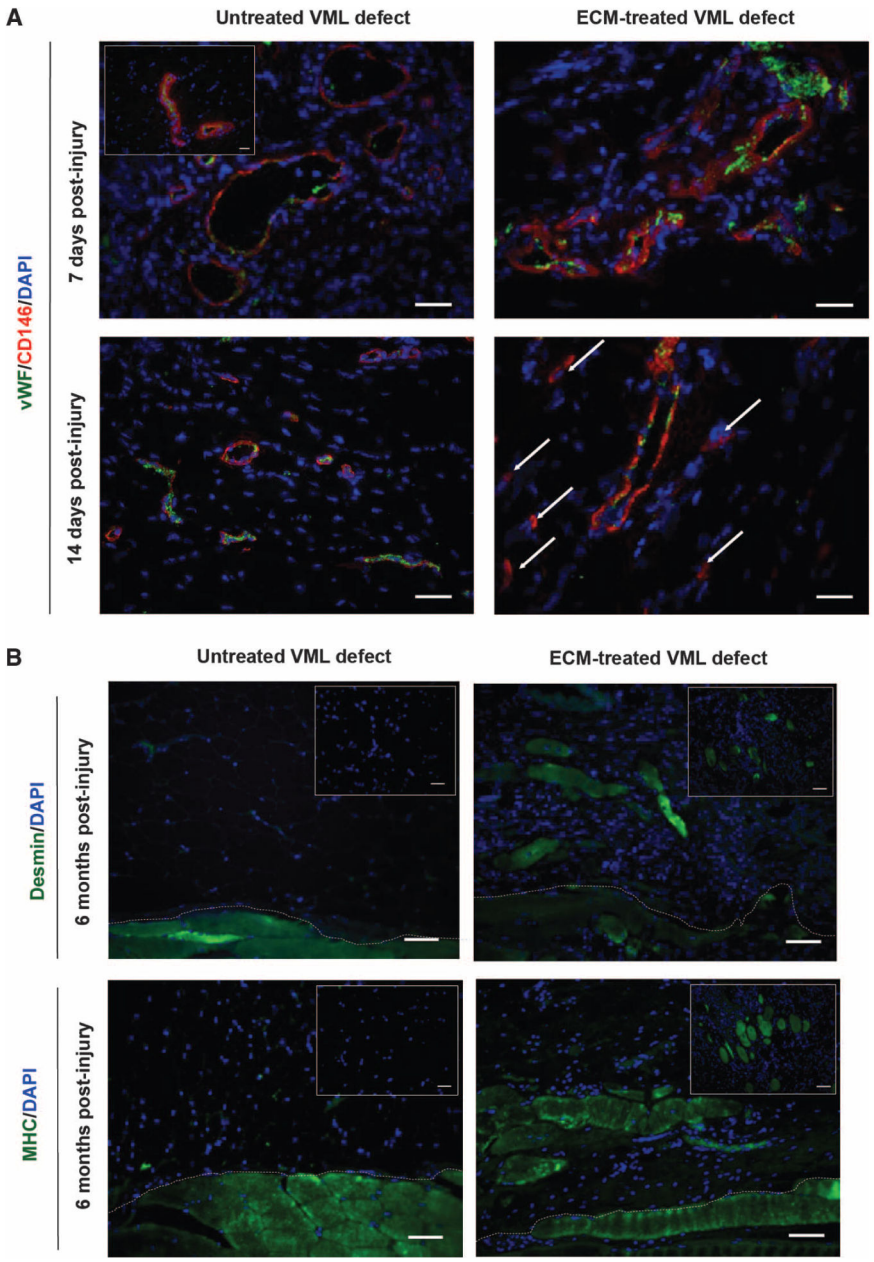

Fig. 1. Progenitor cells are present at the site of ECM scaffolds surgically placed within sites of mouse VML injury

(**A**) CD146$^+$ PVSCs remained in their normal anatomic location, surrounding vascular structures (identified by vWF) at 7 days after injury in both untreated and ECM-treated defects in a mouse model of VML. Healthy, normal mouse skeletal tissue is shown in inset. After 14 days, PVSCs maintained their vascular association in untreated VML defects; conversely, in ECM-treated defects, CD146$^+$ PVSCs were present outside their normal niche (arrows). (**B**) Untreated defects from the mouse model of VML showed no signs of skeletal muscle formation (desmin$^+$, MHC$^+$ cells), whereas ECM scaffold–treated defects showed desmin$^+$, MHC$^+$, and striated skeletal muscle cells at 6 months after injury. Skeletal muscle

cells were identified along the interface with underlying native tissue (dotted white line) as well as throughout the center of the ECM implantation site (insets). Scale bars, 50 μm. DAPI, 4′,6-diamidino-2-phenylindole; MHC, major histocompatibility complex.

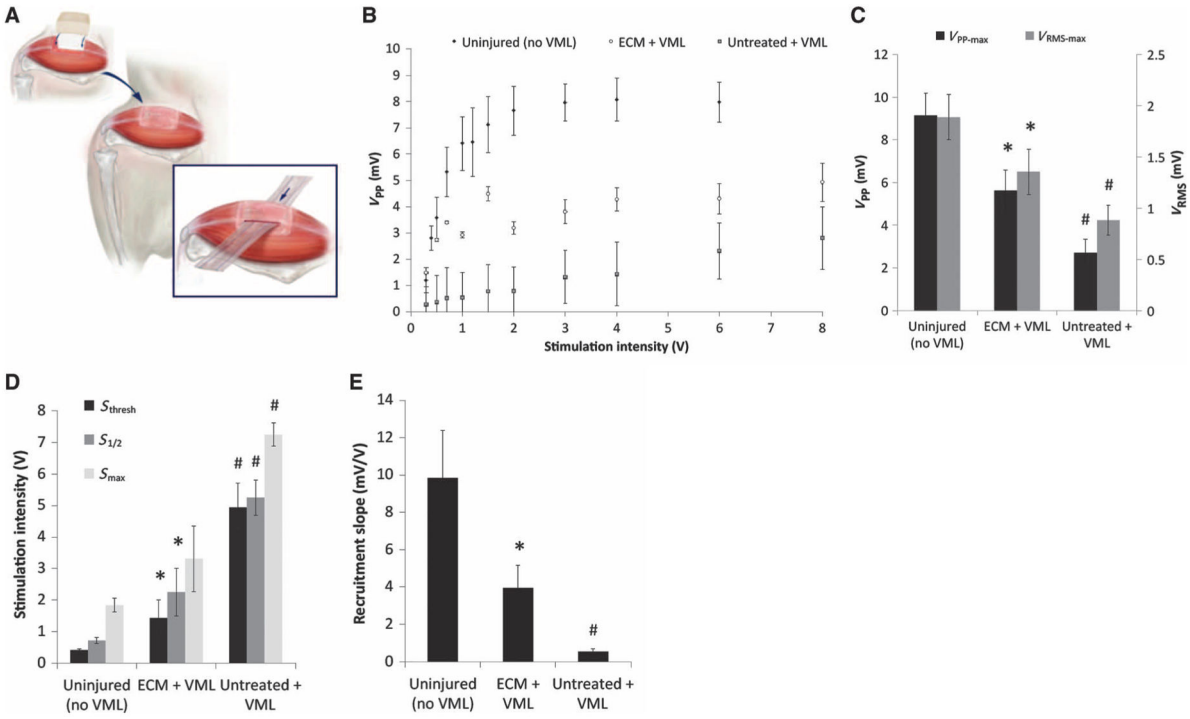

Fig. 2. EMG at 6 months in healthy mouse muscle and in mice with untreated or ECM-treated VML defects

(**A**) Schematic representation of insulated EMG electrode placement within areas of remodeled tissue. (**B**) A range of stimulation intensities was applied to generate muscle recruitment curves from the evoked peak-to-peak voltage (V_{PP}) response. (**C**) Maximal V_{PP} and V_{RMS} responses for each treatment. (**D**) Stimulation intensities required to evoke the minimum CMAP response (S_{thresh}), one-half the maximum response ($S_{1/2}$), and the maximum response (S_{max}) for each treatment group. (**E**) Recruitment rate was calculated as the slope of the recruitment curve at $S_{1/2}$. Data in (B) to (E) are means ± SEM ($n = 8$). $^{*}P < 0.05$ versus untreated, $^{\#}P < 0.05$ versus healthy, Kruskal-Wallis non-parametric analysis of variance (ANOVA) with a post hoc Mann-Whitney U test and Sidak correction.

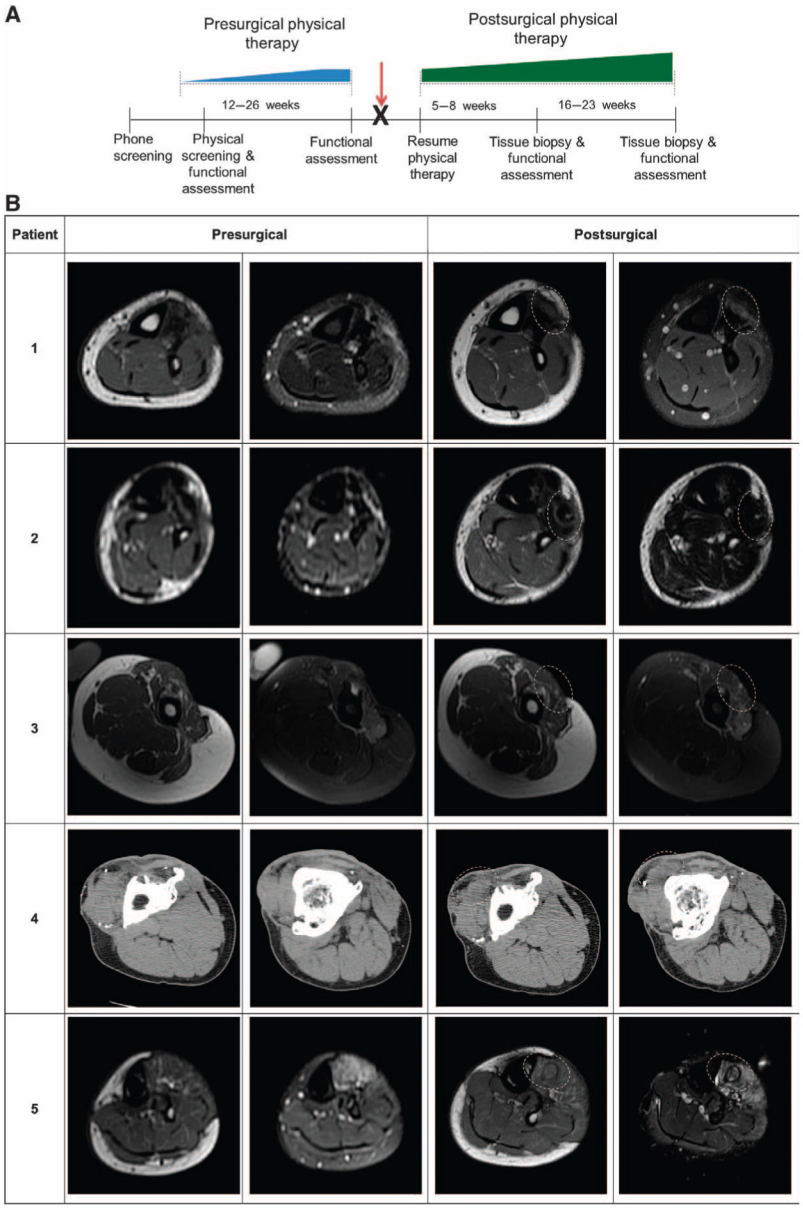

Fig. 3. Study design timeline and imaging of affected extremity before and after surgical implantation in patients

(**A**) All patients completed a customized presurgical physical therapy program that focused specifically on their individual functional deficits and that was designed to maximize their individual potentials before surgical intervention (blue ramp progression, 12 to 26 weeks). The identification and maximization of functional parameters before surgery minimized the likelihood that any improvement after ECM intervention was solely the result of the physical therapy component of care. Patients then underwent the ECM scaffold surgical placement procedure (red arrow) and immediately returned to their presurgical physical therapy regimen (green ramp progression, 5 to 23 weeks). Ultrasound-guided biopsies were taken from the site of ECM scaffold implantation at 5 to 8 weeks for immunostaining. (**B**) Postsurgical images were taken at 6 months. Implantation site is denoted by dotted line.

Patient 1: Pre- and postsurgical axial T1–weighted (left) and fat-saturated T2–weighted (right) MR images of the left distal calf. Patient 2: Presurgical axial T1–weighted (left) and short tau inversion recovery (STIR)–weighted (right); post-surgical axial T1–weighted (left) and T2-weighted (right) MR images of the distal calf. Patient 3: Pre-and postsurgical axial T1 (left) and fat-saturated T2 (right) MR images of the left mid-thigh. Patient 4: Pre- and postsurgical contiguous unenhanced axial CT imaging of the proximal (left) and distal (right) right thigh. Patient 5: Presurgical axial T1 (left) and fat-saturated T2 (right); postsurgical axial T1–weighted (left) and STIR-weighted (right) MR images of the proximal left calf.

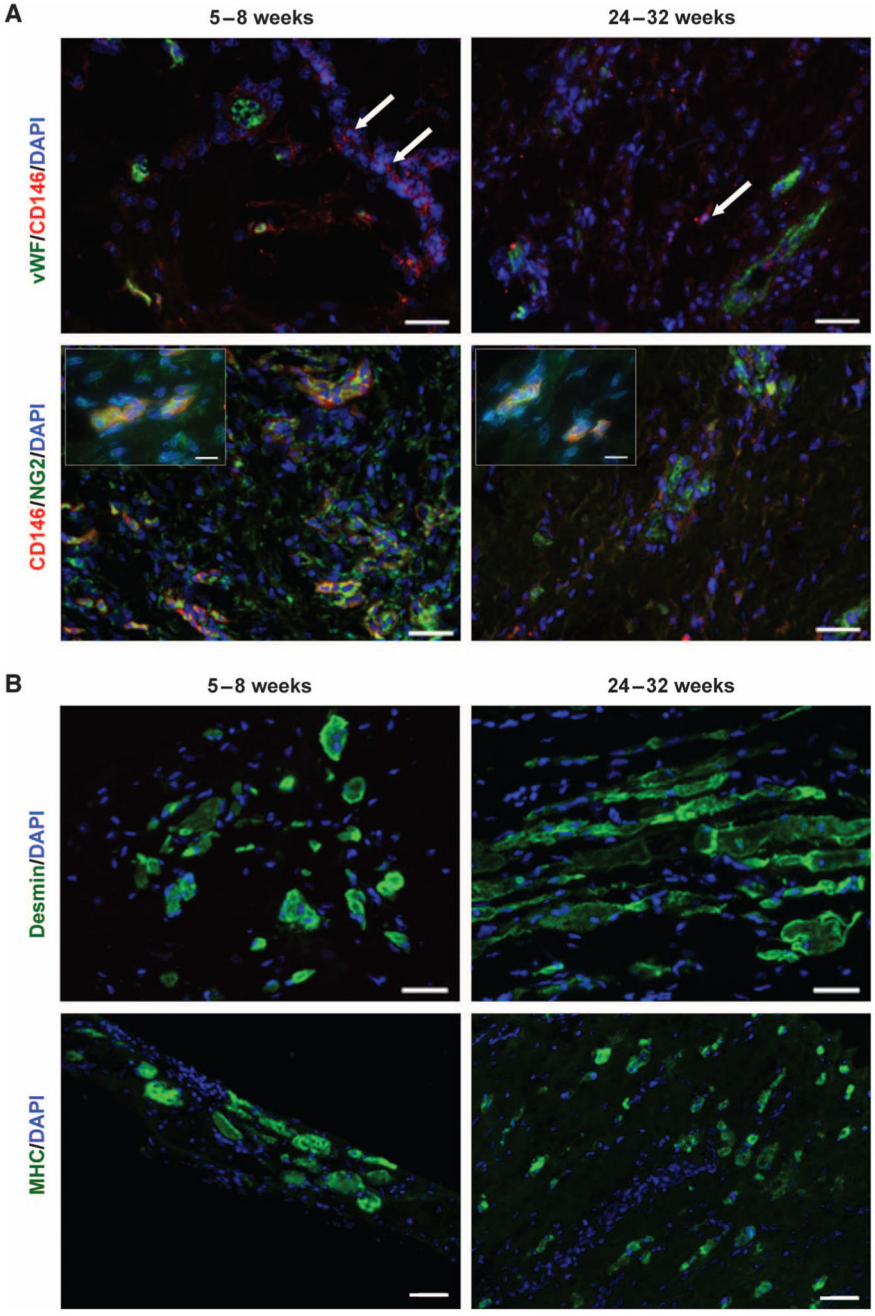

Fig. 4. Constructive tissue remodeling by ECM scaffolds in patients

Representative images are shown here, with images from each patient in fig. S2. (**A**) Biopsied human muscle tissue from ECM-treated VML defects at both 5 to 8 weeks and 24 to 32 weeks after scaffold implantation. PVSCs ($CD146^{+}NG2^{+}$) were present both within and outside of (arrows) their normal perivascular association (vWF^{+} regions). High-magnification insets show colocalization of CD146 and NG2 (inset scale bars, 10 μm). Scale bars, 50 μm. (**B**) Human muscle biopsies from the site of scaffold implantation at 5 to 8

weeks and 24 to 32 weeks after ECM scaffold implantation showed the formation of islands of desmin$^+$ muscle cells. Scale bars, 50 μm.

Table 1

Patient information

Relevant information from each patient ($n = 5$) in the present study. Tissue deficit estimated from MRI or CT scan. IED, improvised explosive device.

Patient	Sex	Age (years)	Injury site (side)	Cause of injury	Time since injury (months)	Previous surgeries	Tissue deficit (estimate)	Status
1	M	34	Anterior tibial compartment (left)	Exercise-induced	13	5	58%	Military
2	M	37	Anterior tibial compartment (left)	Skiing accident	32	4	67%	Civilian
3	M	28	Quadriceps (left)	IED blast	18	14	68%	Military
4	M	27	Quadriceps (right)	IED blast	89	50	83%	Military
5	M	32	Anterior/lateral tibial compartment (left)	Skiing accident	85	8	90%	Civilian

Table 2

Cellular composition of patient biopsies at two different time points after surgery

Semiquantitative findings of $CD146^+NG2^+$ PVSCs and $desmin^+$ muscle cells in patient biopsies at 5 to 8 weeks and 24 to 32 weeks after surgery. Angiogenesis was evaluated by the presence of vWF^+ vasculature structures. $CD146^+NG2^+$ PVSCs were identified independent of $CD31^+$ vessels. $Desmin^+$ cells identified the presence of skeletal muscle cells. −, absent; +, few isolated cells; ++, moderate number of cells or small clusters; +++, large numbers of cells or large cell clusters.

Patient	First biopsy					Second biopsy				
	Weeks after surgery	Number of tissue samples	Angiogenesis	$CD146^+NG2^+$ cells independent of vessels	$Desmin^+$ cells	Weeks after surgery	Number of tissue samples	Angiogenesis	$CD146^+NG2^+$ cells independent of vessels	$Desmin^+$ cells
1	5	7	+++	+	−	24	6	+++	+++	++
2	6	6	++	++	−	26	6	++	−	+++
3	6	8	+	+++	++	26	9	+	−	+
4	8	8	+	−	−	32	8	++	+	+++
5	8	5	+++	++	+	27	8	++	+	++

Table 3

Force production data from each patient

Strength measures as assessed with a handheld dynamometer from each patient. Data are percent change from presurgical maximum obtained after physical therapy.

Patient	Activity	6–8 weeks postsurgical (%)	10–12 weeks postsurgical (%)	24–28 weeks postsurgical (%)
1	Dorsiflexion	0.0	0.0	0.0
2	Dorsiflexion	0.0	0.0	0.0
3	Knee extension	−10.0	18.3	20.0
4	Knee extension	127.9	149.2	136.1
5	Dorsiflexion	−33.3	16.7	33.3
	Average	16.92	36.84	37.88
	SEM	28.4	28.4	25.3

Table 4
Functional task data from each individual patient

Functional measures as assessed by task/exercise completion from each patient. Data are percent change from presurgical maximum obtained after physical therapy. Bold and italicized texts represent positive and negative changes, respectively. Underlined text shows no change from presurgical maximum.

Patient	Activity	6–8 weeks postsurgical (%)	10–12 weeks postsurgical (%)	24–28 weeks postsurgical (%)
1	Single leg stance (s)			
	Eyes open	0.0	0.0	0.0
	Eyes closed	**50.4**	*−81.2*	*−6.8*
	Get up and go (s)	*−4.0*	*−2.0*	*−14.0*
2	Single leg stance (s)			
	Eyes open	0.0	0.0	0.0
	Eyes closed	*−20.1*	**88.7**	**120.1**
	Stork balance test (s)	**33.3**	**41.7**	**26.7**
	Single leg jump landing (inches)	**14.5**	**18.3**	**8.5**
	Triple hop test (inches)	**5.1**	**8.2**	**6.4**
	Functional reach test (inches)			
	Forward	**12.0**	**32.1**	**56.1**
	Backward	**90.8**	**108.8**	**114.1**
3	Single leg hop (inches)	**1980.0**	**2460.0**	**1820.0**
	Single leg squats (repetitions)	0.0	**100.0**	**400.0**
4	Single leg hop (inches)	*−37.5*	**25.0**	**18.8**
	Chair lift test (repetitions)	**84.2**	**273.7**	**323.7**
	Single leg squats (repetitions)	**100.0**	**316.7**	**416.7**
	Triple hop test (inches)	*−21.2*	*−8.7*	**7.7**
5	Single leg stance (s)			
	Eyes open	**232.1**	**232.1**	**232.1**
	Eyes closed	0.0	**20.0**	**85.0**
	Stork balance test (s)	0.0	0.0	**180.0**
	Single leg jump landing (inches)	**400.0**	**783.3**	**1050.0**
	Triple hop test (inches)	**49.5**	**115.4**	**122.0**
	Functional reach test (inches)			
	Forward	**12.0**	**24.0**	**28.0**
	Backward	**33.3**	**66.7**	**83.3**